JOURNAL OF MATERIALS SCIENCE 28 (1993) 1957–1962

Phase transformations and structure–property relationships in a rapidly solidified Ni–Al–Mo alloy

Part II *Structure–property relationships*

SANG YUL LEE*, P. NASH
Illinois Institute of Technology, Chicago, IL 60616, USA

In Part I the complex phase transformations occurring on ageing a melt-spun Ni–Al–Mo–V–Re alloy were determined by transmission electron microscopy (TEM). In the present paper, electrical resistivity and microhardness measurements on the aged, melt-spun ribbon are reported and correlated with the TEM studies. An initial increase in electrical resistivity on ageing corresponds to the spinodal ordering transformation. This is followed by precipitation of α(Mo). This also gives rise to an increase in microhardness with ageing time. The activation energy for this process was determined to be 270.8 kJ mol^{-1}, corresponding to the volume diffusion of Mo in Ni. At long ageing times the electrical resistivity reaches a constant value and the microhardness decreases as the precipitates coarsen and a discontinuous precipitation reaction takes place.

1. Introduction

The complex phase transformation behaviour in an Ni–13.5 at % Al–19.2 at % Mo–1.9 at % V–0.4 at % Re alloy on isothermal ageing below 1000 °C has been discussed previously [1, 2]. Both homogeneous and heterogeneous transformations were observed in this alloy. Briefly, in the early stage of ageing the supersaturated alloy transformed through a homogeneous transformation mechanism (spinodal ordering), followed by several concomitant and/or sequential heterogeneous transformations. A part of the complexity in the transformation behaviour was due to a discontinuous transformation in the grain boundary regions, which developed at the same time as a homogeneous nucleation and growth transformation was occurring in the cells. Also, the appearance of coherent phases such as γ′ (Ni_3Al), metastable Ni_2Mo and metastable $Ni_3Mo(D0_{22})$ phases increases the complexity. At one stage eight different phases co-exist in this alloy.

In order to gain further insight into the transformation behaviour of this alloy, electrical resistivity and microhardness measurements were made and correlated with the microstructural evidence presented in Part I [2].

2. Experimental procedure

The methods of sample preparation and heat treatment were described previously [1, 2]. Ribbons 4 cm in length for the electrical resistivity testing and ribbons 2 cm in length for the microhardness testing were cut from the as-cast ribbons. The electrical resistance of the 4 cm long ribbon was measured and recorded prior to encapsulation.

Before heat treatment, the electrical resistance of the as-cast ribbons was measured and recorded, so that samples with consistent readings, with no more than 5% deviation from the average reading, were used for the heat treatment. The electrical resistance of the as-cast ribbons varied depending upon several factors such as thickness, width, and solid-state cooling after rapid solidification. A four-probe Keithley Model 580 micro-ohmmeter with a resolution of 10 μΩ was used to measure the electrical resistance of the specimen in a custom-built jig [3]. The average electrical resistance of the aged specimen, ρ_t, was used to calculate the electrical resistivity ratio (ERR), ρ_t/ρ_o, using the previously measured electrical resistance of the as-cast specimen, ρ_0.

The microhardness was measured on cold-mounted samples using a Buehler microhardness tester with a load of 100 g applied for 10 s to the centre region of the cross-section of the specimen. At least 12 readings were made from each specimen, the maximum and minimum readings were discarded and the rest of the readings were converted into diamond pyramid hardness values (DPH). The average hardness was calculated for each sample.

The physical and mechanical property measurements were correlated with the corresponding microstructure discussed in Part I [2] so that a more comprehensive description of the ageing behaviour of this alloy could be made.

* *Present address*: KIMM, 66 Sangnam-Dong, Changwon, Kyungnam, South Korea.

0022–2461

3. Results and discussion

3.1. Electrical resistivity measurements

The primary purpose of the electrical resistivity measurements was to follow the microstructural transformation sequence by correlating the electrical resistivity results with microstructural observations and thereby deduce information on the kinetics. The electrical resistivity ρ_t was measured as a function of ageing time and ageing temperature and the ERR, ρ_t/ρ_o, determined where ρ_o is the resistivity of the as-cast material. The results are presented in Fig. 1a as a function of ageing time at different temperatures.

The ERR curve consists of three regions. There is an initial increase in ERR up to a maximum (region I), then a rapid drop in ERR (region II) followed by a levelling-off region.

In region I, the ERR increases as ageing time increases. Examination of the structural developments in region I showed that there was a transformation of the completely supersaturated disordered f.c.c. γ(Ni) matrix with short-range ordering (SRO) into a mixture of γ(Ni) and $\gamma'(Ni_3Al)$ by a spinodal ordering mechanism which produced a finely spaced modulated structure in the cells (see Fig. 1 and Fig. 4 in Part I [2]). Hence, the initial increase of the ERR can be explained by the development of a composition/order parameter modulated structure which decreases the electron mean free path. As ageing begins, the supersaturated matrix begins to lower its free energy initially by developing short modulation wavelengths, 3.1 nm after ageing for 1 min at 650 °C. As ageing time increases the modulation wavelength also increases (3.2 and 3.75 nm after ageing for 5 min at 650 and 700 °C, respectively), resulting in a continuing increase in ERR. An increase in the electrical resistivity due to spinodal ordering in Ni–Mo–Cr alloys has been reported previously [4]. As ageing proceeds, however, the precipitation of α(Mo) in the cells begins to occur, leading to a decrease in supersaturation of the matrix which results in a decrease in the ERR. Because the effect of solute on ERR is very strong the α(Mo) precipitation leads to a rapid decrease in ERR which overwhelms any tendency to increase ERR due to the coarsening of the spinodal structure. The compensating effects from both spinodal ordering and α(Mo) precipitation gives rise to a maximum in the ERR curves. As ageing temperature increases, the time to reach the maximum as well as the magnitude of the increase in ERR decreases. In fact, at 800 and 750 °C the specimen shows only a very small increase in the ERR at the maximum. This decrease in the maximum ERR and in the time to reach the maximum at higher temperatures is due to the faster kinetics of α(Mo) precipitation. For example, the ribbon aged at 700 °C and exhibiting α(Mo) precipitate at the cell boundaries (Fig. 2) showed a lower maximum in ERR than that aged at 650 °C with no α(Mo) precipitate at the cell boundaries [3].

On further ageing, the decrease in the supersatur-

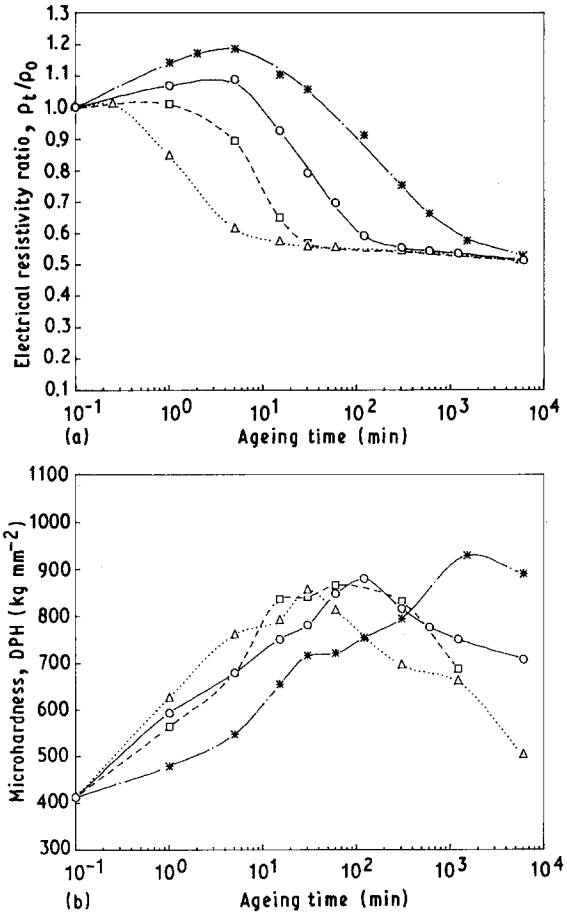

Figure 1 (a) Electrical resistivity ratio and (b) microhardness as a function of ageing time and temperature (*) 650 °C, (○) 700 °C, (□) 750 °C, (△) 800 °C.

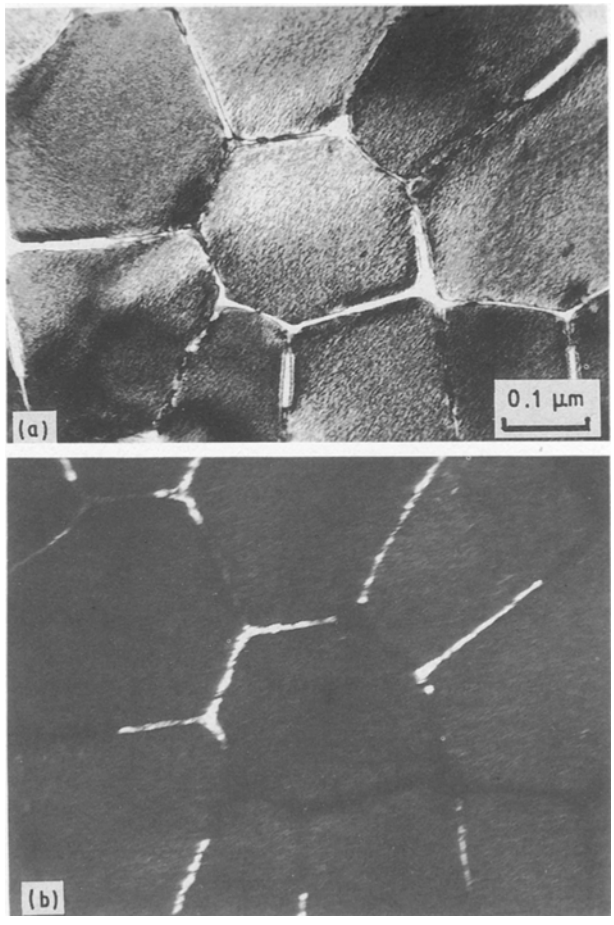

Figure 2 TEM micrographs of ribbon after ageing for 5 min at 700 °C: (a) bright-field image, (b) dark-field image of α(Mo) precipitates at the cell boundaries.

ation in the matrix as well as the precipitation of α(Mo) in the cell boundaries results in a decrease in the ERR. At this stage (region II), the contribution of the modulated structure to the ERR is small relative to the effect of decreasing supersaturation. A rapid drop of the ERR after reaching the maximum occurs in region II until the ERR reaches a plateau at a value of about 0.6 for all ageing temperatures. Microstructural examination of the alloy in region II reveals several transformations occurring simultaneously and sequentially. First of all, α(Mo) precipitates at the cell boundaries, as shown in Fig. 2 (see also Fig. 4 in Part I [2]). This is to be expected because the cell boundaries are fast diffusion paths and a small amount of solute segregation is expected in the cell boundaries during solidification. Also, the activation energy for heterogeneous nucleation in the cell boundaries is smaller than for nucleation in the cell. In the meantime, in the cells, the modulated structure already present is developing further [2] and α(Mo) precipitates with a plate-like morphology begins to form (see Fig. 5c in Part I [2] as indicated by arrow). The plate-like α(Mo) precipitates gradually increase in volume fraction as ageing time increases.

Also in region II, discontinuous transformation at the grain boundaries was observed, in which the highly strained matrix transformed to disc-shaped α(Mo) in a strain-free γ′(Ni_3Al) matrix (see Fig. 5 in Part I [2]). In addition the precipitation of two metastable phases, Ni_2Mo and $Ni_3Mo(D0_{22})$, is observed toward the end of region II after 120 min at 700 °C (Fig. 7 in Part I and Fig. 3 of this paper for specimen 5/800). The precipitation of the metastable phases does not seem to affect the ERR and this is probably due to their small volume fractions. The homogeneous nucleation and growth of the plate-like α(Mo) precipitates continues until the supersaturation of Mo has been reduced to a low level, resulting in the ERR reaching the end of region II. Further ageing results in the precipitates starting to coarsen and region III in the ERR plot results. By examining ribbons with similar ERR values but different ageing temperatures, it was noted that the microstructures and diffraction patterns of ribbons with similar ERR values look very similar. For example, the microstructure of the 5/700 ribbon (Fig. 2) and the SADP of the 5/800 ribbon are very similar to those of 30/650 (Fig. 4) and 120/700 (Fig. 7 in Part I). Assuming that similar microstructures developed at different ageing times and temperatures have similar ERRs, the ERR can be related to a simple rate equation as shown below:

$$\frac{d(\rho_t/\rho_0)}{dt} \propto \exp(-Q/RT)$$

The time to reach a certain ERR value at different temperatures was determined from Fig. 1a and the log of the inverse of time in seconds to reach the ERR value was plotted as a function of the inverse of the absolute temperature (Fig. 4). The plot shows a good linear fit for different ERR values. From the slopes of these lines, the apparent activation energy of the rate-controlling process in region II was calculated to be $270.8 \pm 2.0\ kJ\ mol^{-1}$. This activation energy is very close to the activation energy for the volume diffusion of Mo in Ni, $269.2\ kJ\ mol^{-1}$ [5]. Although two major transformations occur in region II, the calculated activation energy suggests that the mechanism for the change in ERR is controlled by the homogeneous precipitation of the plate-like α(Mo) phase rather than the discontinuous transformation. In fact, the contribution of the discontinuous transformation to the decrease in ERR in region II is likely to be negligible because the amount of the ERR change in region III, where the discontinuous transformation continues to proceed, is very small. Also, the shape of the ERR curve, showing an abrupt change in slope, implies the beginning and end of a transformation.

In region III, the ERR tends to level-off gradually. On further ageing the ERR reaches a similar value for all of the ageing temperatures. The microstructural features in this region include growth of the discontinuously transformed regions and a general coarsening of α(Mo), both in the discontinuously transformed regions and within the cells (Figs 5 and 6). In addition the metastable phase transformations as well as the formation of orthorhombic Ni_3Mo phase (see Fig. 11 in Part I [2]) were observed; however, these changes affect the ERR very little.

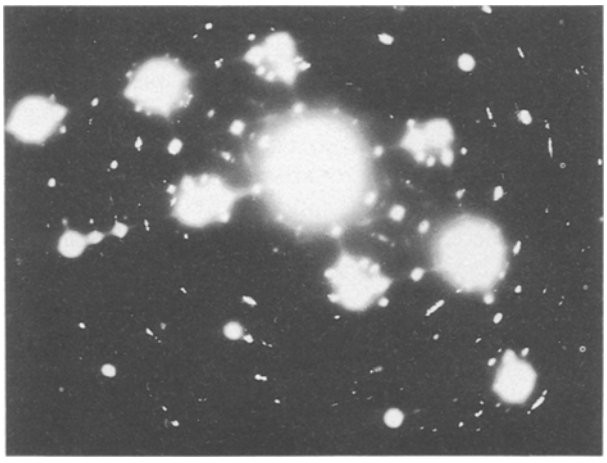

Figure 3 Selected-area diffraction pattern of ribbon after ageing for 5 min at 800 °C, [0 0 1] zone.

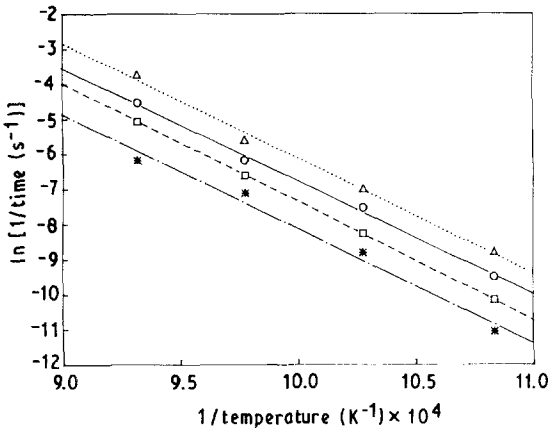

Figure 4 Relationship between time to reach certain ERR value and temperature: ρ_t/ρ_0 = (*) 0.6, (□) 0.7, (○) 0.8, (△) 0.9.

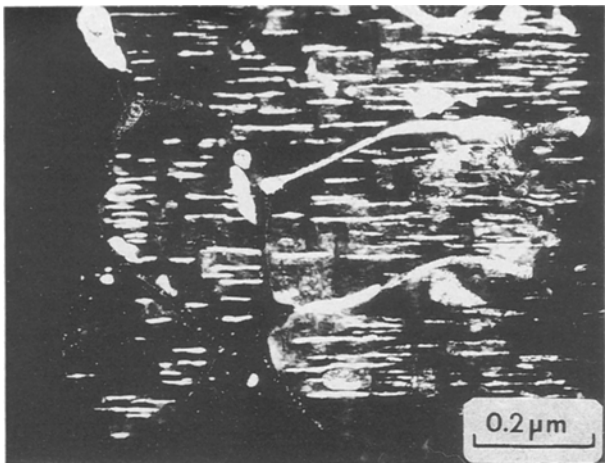

Figure 5 Dark-field image of coarsened α(Mo) precipitates after ageing for 600 min at 700 °C.

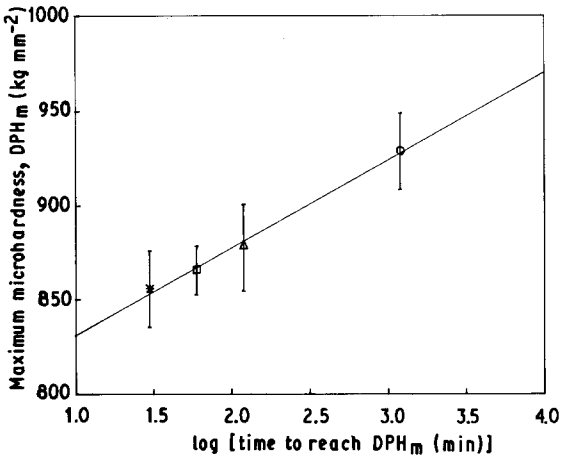

Figure 7 Maximum microhardness (DPH_m) at different temperature as a function of log (ageing time): (○) 650 °C, (△) 700 °C, (□) 750 °C, (*) 800 °C.

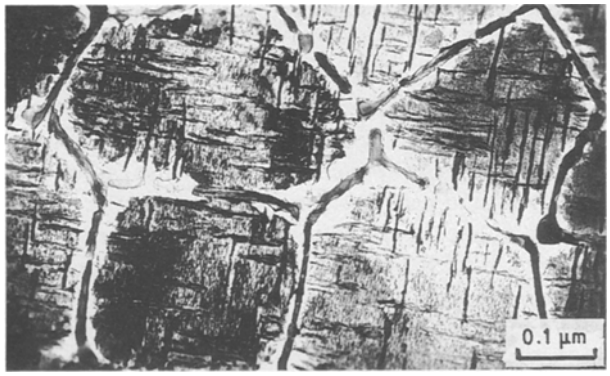

Figure 6 TEM micrograph of ribbon after ageing for 300 min at 700 °C.

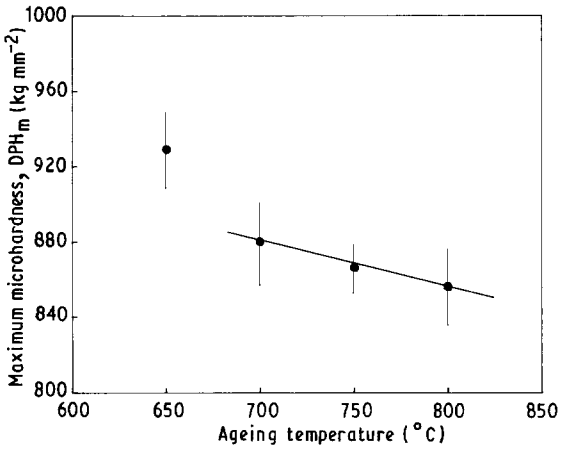

Figure 8 Maximum microhardness (DPH_m) as a function of ageing temperature.

3.2. Microhardness measurements

The average diamond-pyramid hardness number (DPH) of as-cast and aged specimens was determined. The results as a function of ageing time for different temperatures are summarized in Fig. 1b. Generally the curves show the classic precipitation-hardening behaviour observed for ageing of supersaturated solid solutions. The maximum hardness and the time to reach the maximum hardness increase as the ageing temperature decreases.

Close examination reveals that the maximum hardness is linearly proportional to the ageing time as temperature decrease (Fig. 7). From this relationship the following empirical equation was obtained:

$$DPH_m = 784.7 + 46.5 \log t_m \quad (1)$$

where DPH_m is the maximum microhardness achieved at different temperatures and t_m is the ageing time in minutes to reach DPH_m.

The DPH_m as a function of ageing temperature is given in Fig. 8 and shows a linear relationship with ageing temperature above 700 °C. This relationship can be represented by

$$DPH_m = 1039.5 - 0.23\ T \qquad T > 700\,°C \quad (2)$$

where T is the ageing temperature (°C). Thus the approximate DPH_m and t_m of this alloy can be estimated at temperatures higher than 700 °C at least up to 800 °C, using Equations 1 and 2. The DPH_m at 650 °C is much higher than predicted by this relationship.

On ageing, the microhardness of the as-cast alloy increases by a factor of 2 to 2.5. This large increase can be attributed to several strengthening mechanisms developed on ageing. In the as-cast state, the microhardness can be related to the fine cell size and solid-solution strengthening. On ageing, fine precipitates of γ′(Ni_3Al) form by spinodal ordering and the high coherency strain energy associated with the γ′(Ni_3Al) gives rise to a large microhardness increase at the early stage of ageing. This is followed by α(Mo) precipitation at the cell boundaries and the precipitation of plate-like α(Mo) in the cells which causes further strengthening. At a later stage, the metastable phases precipitate and these are expected to contribute to strengthening to a small extent. Nemoto *et al.* [6, 7] have reported a strengthening effect from the metastable Ni_2Mo phase in directionally solidified Ni–Al–Mo alloy. Each precipitate described above is believed to contribute to some extent, resulting in a high microhardness. However, it is difficult to identify

the amount of strengthening from each constituent quantitatively, because the precipitation processes overlap one another. There are also processes that would be expected to decrease the microhardness of the alloy as ageing proceeds. These include (i) depletion of the supersaturation in the matrix, (ii) the discontinuous transformation at the grain boundaries, and (iii) precipitate coarsening.

For the same temperature difference, a much larger increment of DPH_m between 650 and 700 °C was observed than between other temperatures (Fig. 7). Assuming that the major strengthening effect comes from the precipitation of plate-like α(Mo), the strengthening effects at different temperatures can be qualitatively related to the volume fraction of the precipitate (i.e. variation of the equilibrium solute concentrations at different temperatures). Since the difference in DPH_m between 700 and 800 °C is smaller than that between 650 and 700 °C, it is possible that an abrupt change in solvus slope between 650 and 700 °C occurs implying an invariant reaction between 650 and 700 °C or the crossing of a phase boundary. Examining the microstructural developments on ageing, the orthorhombic Ni_3Mo phase was observed at 700 and 800 °C, but not at 650 °C, which supports the proposition of crossing a phase boundary.

It is also noted that the microhardness changes for 650 °C ageing reach a plateau before increasing again to the DPH_m.The probable explanation for this is illustrated in Fig. 9. At an early stage before 5 min at 650 °C the major strengthening effect comes only from the spinodal ordering of the γ(Ni) matrix to γ(Ni)/γ′(Ni_3Al). On further ageing, α(Mo) precipitation will increase the microhardness of the alloy. Since these two processes overlap it is expected that the total microhardness is the sum of these two constituents as shown in Fig. 9. The plateau region may result from the precipitation of α(Mo) occurring when the γ(Ni)/γ′(Ni_3Al) structure begins to over-age or coarsen. This explanation is supported by the co-existence of the α(Mo) precipitates and the modulated structure as shown in Fig. 2 after 5 min at 700 °C. Similar microhardness behaviour due to fine Guinier–Preston zones was observed by Gayler [8, 9] and Hardy and co-workers [10, 11] in Al–Cu alloys aged at 130 °C. Also, the reason that this plateau was not so obvious at higher temperatures was probably due to a faster kinetics, as two strengthening constituents tended to reinforce each other.

In Fig. 1 the ERR and DPH curves are drawn on the same time-scale for direct comparison. The times to reach the maximum hardness at different temperatures correspond to the times for the end of region II. From this fact, in conjunction with the associated microstructure, two important conclusions can be drawn. One is that the major strengthening mechanism of this alloy is the precipitation of the plate-like α(Mo) phase. The other is that the decrease in microhardness after the maximum hardness corresponds to region III in the electrical resistivity curves where general coarsening of the microstructure occurs.

4. Summary and conclusions

The relationship between ρ_t/ρ_0 and ageing time shows three regions. In region I, there is an initial increase of ρ_t/ρ_0 due to spinodal ordering. The increase in resistivity is due to a reduction in the mean free electron path caused by the fine scale of the microstructure. A rapid drop of ρ_t/ρ_0 occurs in region II due to the homogeneous nucleation of plate-like α(Mo). The decrease in resistivity results from the removal of Mo atoms from the solid solution. The activation energy for this process was determined to be 270.8 $kJ\,mol^{-1}$, in good agreement with the value for volume diffusion of Mo in Ni. This is followed by region III where a gradual decrease of ρ_t/ρ_0 is observed due to the general coarsening of the microstructure. The discontinuous transformation at the grain boundaries, the orthorhombic Ni_3Mo phase, and the formation of metastable phases does not significantly affect the electrical resistivity.

The ageing time to reach the maximum hardness at each temperature correlates well with the end of region II, suggesting that most of the strengthening of the alloy is due to the precipitation of the plate-like α(Mo) phase. Empirical relationships for the maximum microhardness, ageing time and ageing temperature were derived.

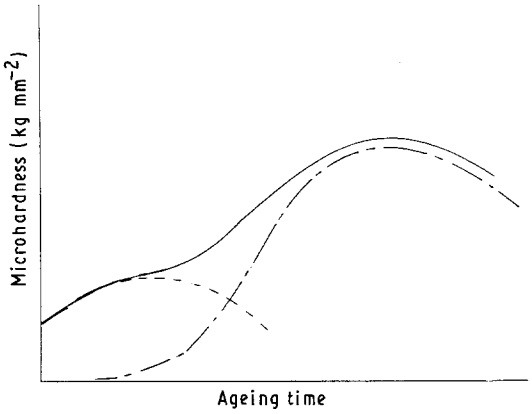

Figure 9 Schematic diagram explaining the double strengthening mechanisms operating at 650 °C. (— · —) ΔDPH_α, (– – –) $\Delta DPH_{\text{spinodal ordering}}$, (——) $DPH = \Delta DPH_\alpha + \Delta DPH_{\text{spinodal ordering}}$.

Acknowledgements

This paper is based on work by S.Y.L. in partial fulfilment of the requirements for the PhD degree at Illinois Institute of Technology. The authors wish to thank the NASA Lewis Research Center for material preparation and also thank Dr Nestor Zaluzec and Mr Russ Cook at Argonne National Laboratory for provision of TEM facilities. One of the authors (S.Y.L) gratefully acknowledges financial support provided by the Department of Metallurgical and Materials Engineering at Illinois Institute of Technology.

References

1. S. Y. LEE, P. NASH and S. BRADLEY, *J. Mater. Sci.* **25** (1990) 1219.
2. S. Y. LEE and P. NASH, *ibid.* **28** (1993) 1946.

3. S. Y. LEE, PhD thesis, Illinois Institute of Technology (1988).
4. K. VASUDEVAN and E. STANSBURY, *Scripta Metall.* **19** (1985) 1101.
5. E. BRANDES, "Smithells Metals Handbook", 6th Edn (Butterworth, London, 1983) p. 13.
6. M. NEMOTO, T. HONDA, Y. NAKAGAWA, Y. SAIGA and H. SUTO, *Trans. Jap. Inst. Met.* **21** (1980) 495.
7. *Idem, ibid.* **21** (1980) 505.
8. M. GAYLER, *J. Inst. Metals* **66** (1940) 67.
9. *Idem, ibid.* **72** (1946) 243.
10. H. HARDY, *ibid.* **19** (1951) 321.
11. J. SILCOCK, T. HEAL and H. HARDY, *ibid.* **82** (1953–54) 239.

Received 8 May
and accepted 11 June 1992